Syntheses, Crystal Structures and Properties of New Lead(II) or Bismuth(III) Selenites and Tellurite

Su-Yun Zhang,[a, b] Chun-Li Hu,[a] Pei-Xin Li,[a] Hai-Long Jiang,[a] Jiang-Gao Mao*,[a]

Table S1. State Energies (eV) of the L-CB and the H-VB of the title compounds.

Figure S1.Energy-dispersive X-ray spectroscopy of $Pb_3(TeO_3)Cl_4$ (a), $Pb_3(SeO_3)_2Br_2$ (b), $Pb_2Cd_3(SeO_3)_4I_2(H_2O)$ (c), $Pb_2Ge(SeO_3)_4$ (d) and $BiFe(SeO_3)_3$ (e).

Figure S2. Simulated and experimental XRD powder patterns for $Pb_3(TeO_3)Cl_4$ (a), $Pb_3(SeO_3)_2Br_2$ (b), $Pb_2Cd_3(SeO_3)_4I_2(H_2O)$ (c), $Pb_2Ge(SeO_3)_4$ (d) and $BiFe(SeO_3)_3$ (e).

Figure S3. IR Spectra of $Pb_3(TeO_3)Cl_4$ (a), $Pb_3(SeO_3)_2Br_2$ (b), $Pb_2Cd_3(SeO_3)_4I_2(H_2O)$ (c), $Pb_2Ge(SeO_3)_4$ (d) and $BiFe(SeO_3)_3$ (e).

Figure S4. Absorption spectra of $Pb_3(TeO_3)Cl_4$ (a), $Pb_3(SeO_3)_2Br_2$ (b), $Pb_2Cd_3(SeO_3)_4I_2(H_2O)$ (c), $Pb_2Ge(SeO_3)_4$ (d) and $BiFe(SeO_3)_3$ (e).

Figure S5. Optical diffuse reflectance spectra of $Pb_3(TeO_3)Cl_4$ (a), $Pb_3(SeO_3)_2Br_2$ (b), $Pb_2Cd_3(SeO_3)_4I_2(H_2O)$ (c), $Pb_2Ge(SeO_3)_4$ (d) and $BiFe(SeO_3)_3$ (e).

Figure S6. The orientations of the TeO_3 in $Pb_3(TeO_3)Cl_4$ and that of SeO_3 in $BiFe(SeO_3)_3$.

Figure S7. Plots of χ_M *vs.* T (a) and $\chi_M T$ *vs.* T (b) at various fields in 2-50 K.

Figure S8. Band structures for $Pb_3(TeO_3)Cl_4$ (a), $Pb_3(SeO_3)_2Br_2$ (b), $Pb_2Cd_3(SeO_3)_4I_2(H_2O)$ (c), $Pb_2Ge(SeO_3)_4$ (d) and $BiFe(SeO_3)_3$ (e). The Fermi level is set at 0 eV.

Figure S9. Total density of states and partial density of states of $Pb_3(TeO_3)Cl_4$ (a), $Pb_3(SeO_3)_2Br_2$ (b), $Pb_2Cd_3(SeO_3)_4I_2(H_2O)$ (c), $Pb_2Ge(SeO_3)_4$ (d) and $BiFe(SeO_3)_3$ (e). The Fermi level is set at 0 eV.

Figure S10. The TGA diagram of $Pb_2Cd_3(SeO_3)_4I_2(H_2O)$ and the enlarged TGA diagram between 30-120 °C.

Table S1. State Energies (eV) of the L-CB and the H-VB of the title compounds.

$Pb_3(TeO_3)Cl_4$	k-point	L-CB	H-VB
(0.000 0.000 0.000)	G	3.203994	0
(0.000 0.000 0.500)	Z	3.453067	-0.21098
(-0.500 0.000 0.500)	T	3.48125	-0.27873
(-0.500 0.000 0.000)	Y	3.550821	-0.25144
(-0.500 0.500 0.000)	S	3.614462	-0.29215
(0.000 0.500 0.000)	X	3.233923	-0.02905
(0.000 0.500 0.500)	U	3.492213	-0.22996
(-0.500 0.500 0.500)	R	3.440201	-0.26489
$Pb_3(SeO_3)_2Br_2$	k-point	L-CB	H-VB
(-0.500 0.000 0.500)	L	3.54169	-0.10655
(-0.500 -0.500 0.500)	M	3.25249	-0.1912
(-0.500 0.000 0.000)	A	3.41066	-0.0158
		3.40714	0
(0.000 0.000 0.000)	G	3.2766	-0.10619
		3.24863	-0.08186
(0.000 -0.500 0.500)	Z	3.54169	-0.10655
(0.000 0.000 0.500)	V	3.57285	-0.12914
$Pb_2Cd_3(SeO_3)_4I_2(H_2O)$	k-point	L-CB	H-VB
(0.000 0.000 0.000)	G	3.11306	0

(0.000 0.500 0.000)	F	3.29865	-0.03482
(0.000 0.500 0.500)	Q	3.30001	-0.11629
(0.000 0.000 0.500)	Z	3.27715	-0.0804
(0.000 0.000 0.000)	G	3.11306	0
$Pb_2Ge(SeO_3)_4$	k-point	L-CB	H-VB
(0.000 0.000 0.500)	Z	3.331244	-0.24005
(0.000 0.000 0.000)	G	3.060881	-0.17644
(0.000 0.500 0.000)	Y	3.396029	-0.11796
(-0.500 0.500 0.000)	A	3.458755	0
(-0.500 0.000 0.000)	B	3.282407	-0.20319
(-0.500 0.000 0.500)	D	3.425304	-0.20556
(-0.500 0.500 0.500)	E	3.596733	-0.03
(0.000 0.500 0.500)	C	3.278143	-0.15612
$BiFe(SeO_3)_3$	k-point	L-CB	H-VB
(0.000 0.000 0.000)	G	0.637083	0
(0.000 0.000 0.500)	Z	0.740137	-0.06755
(-0.500 0.000 0.500)	T	0.837538	-0.09387
(-0.500 0.000 0.000)	Y	0.789921	-0.08692
(-0.500 0.500 0.000)	S	0.951474	-0.13528
(0.000 0.500 0.000)	X	0.837547	-0.05791
(0.000 0.500 0.500)	U	0.923435	-0.05921
(-0.500 0.500 0.500)	R	0.987903	-0.15199

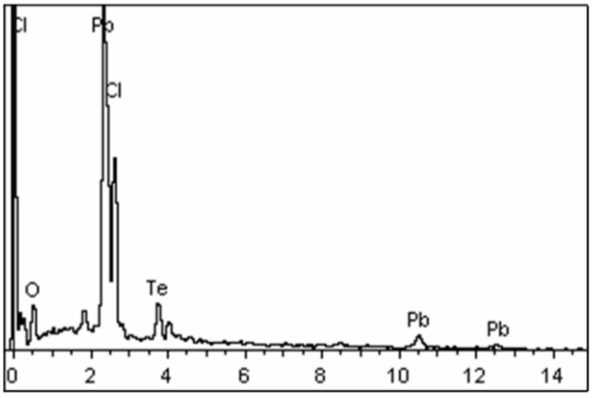

Full scale: 961 cst Cursor: 0.000 KeV

(a)

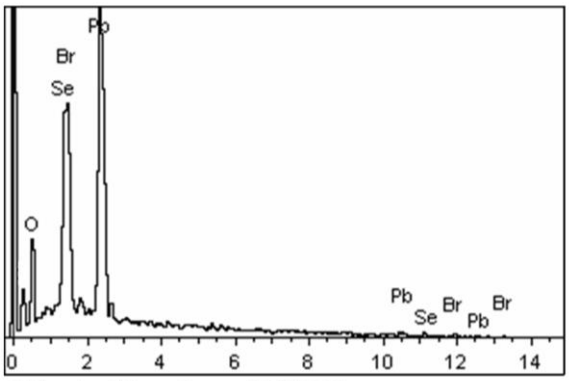

Full scale: 672 cst Cursor: 0.000 KeV

(b)

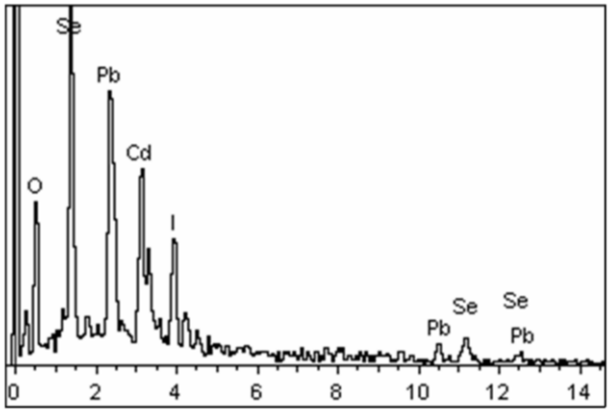

Full scale: 143 cst Cursor: 0.000 KeV

(c)

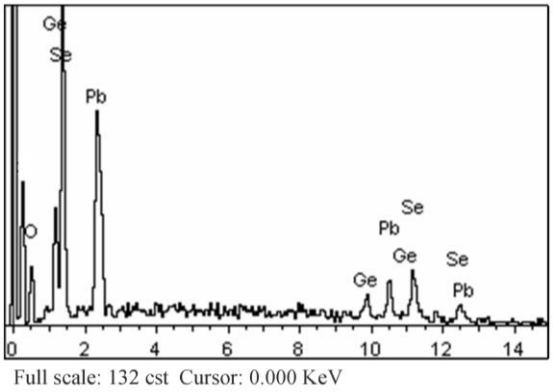

(d)

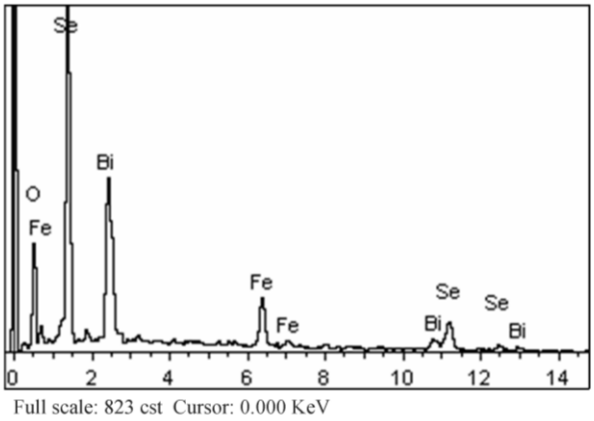

(e)

Figure S1. Energy-dispersive X-ray spectroscopy of $Pb_3(TeO_3)Cl_4$ (a), $Pb_3(SeO_3)_2Br_2$ (b), $Pb_2Cd_3(SeO_3)_4I_2(H_2O)$ (c), $Pb_2Ge(SeO_3)_4$ (d) and $BiFe(SeO_3)_3$ (e).

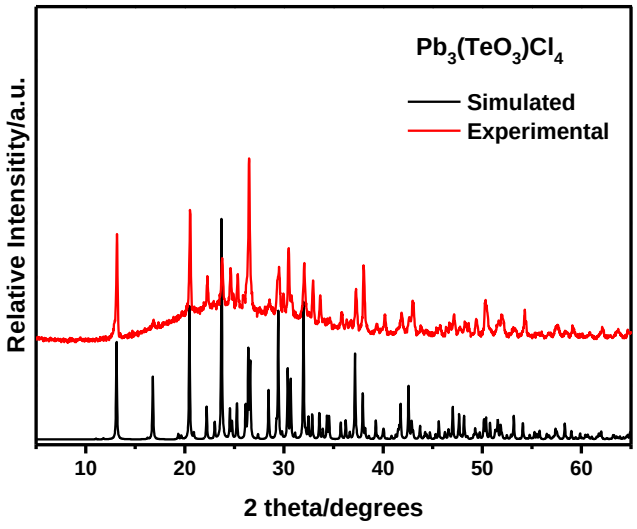

(a)

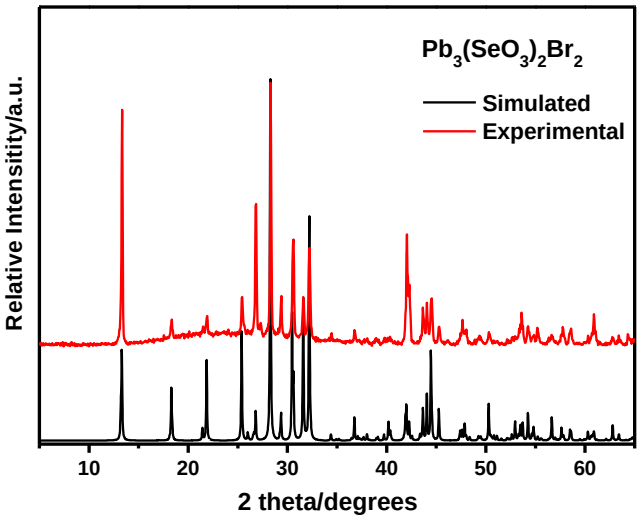

(b)

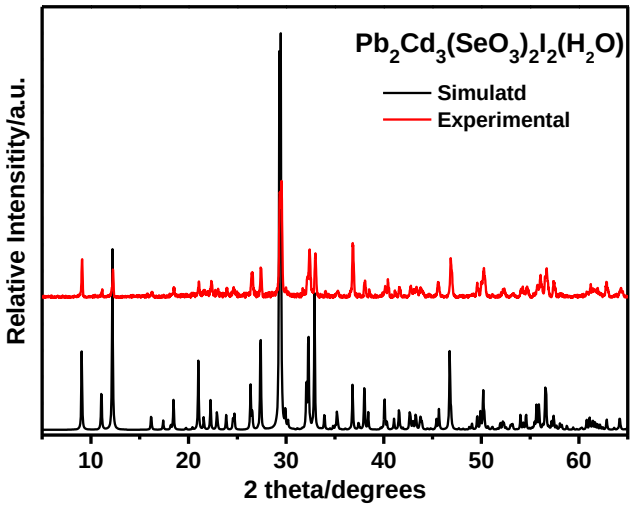

(c)

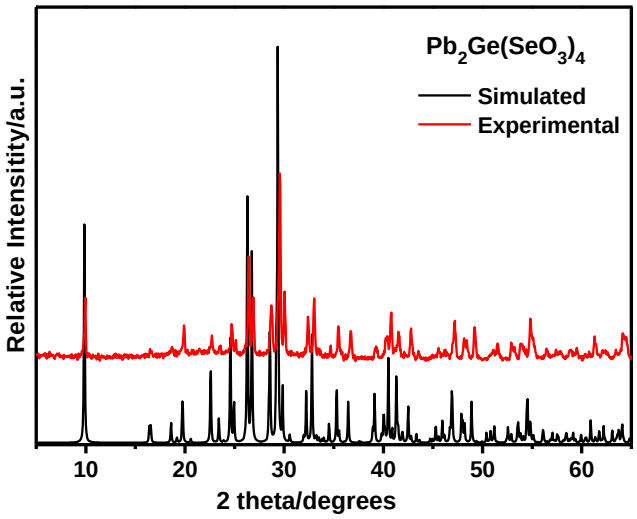

(d)

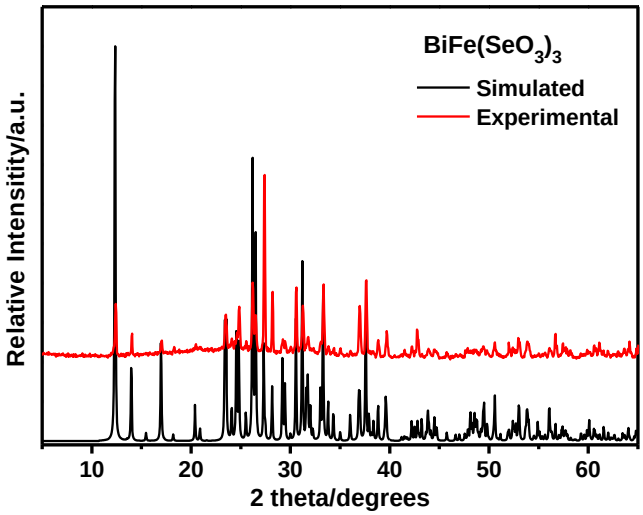

(e)

Figure S2. Simulated and experimental XRD powder patterns for $Pb_3(TeO_3)Cl_4$ (a), $Pb_3(SeO_3)_2Br_2$ (b), $Pb_2Cd_3(SeO_3)_4I_2(H_2O)$ (c), $Pb_2Ge(SeO_3)_4$ (d) and $BiFe(SeO_3)_3$ (e).

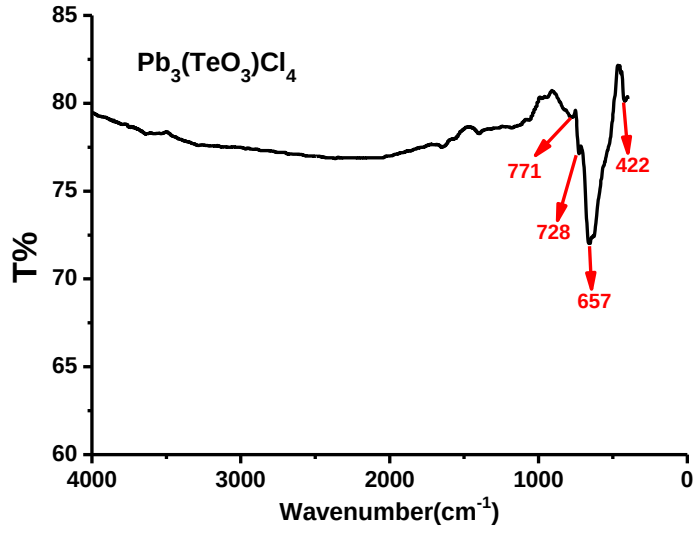

(a)

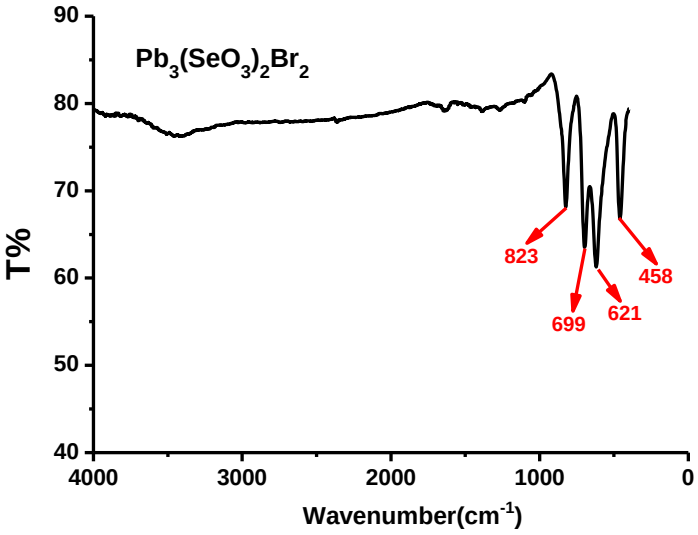

(b)

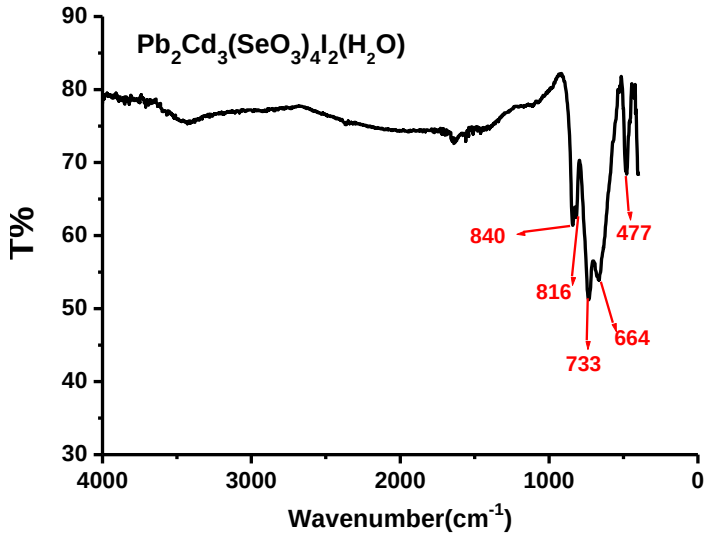

(c)

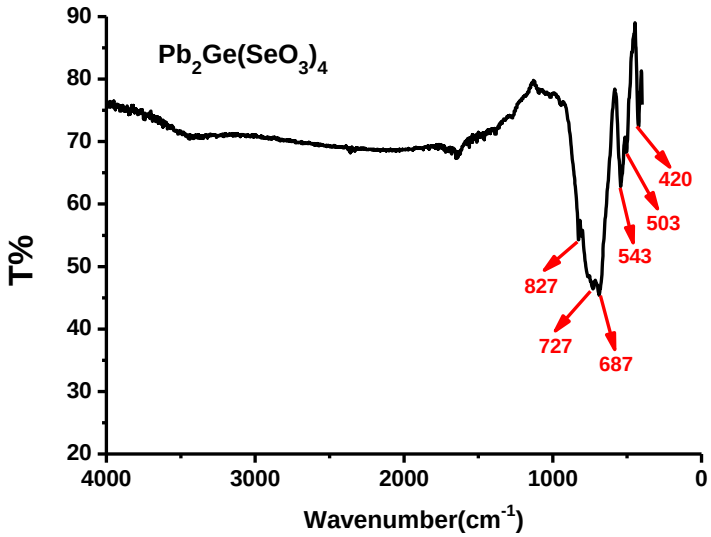

(d)

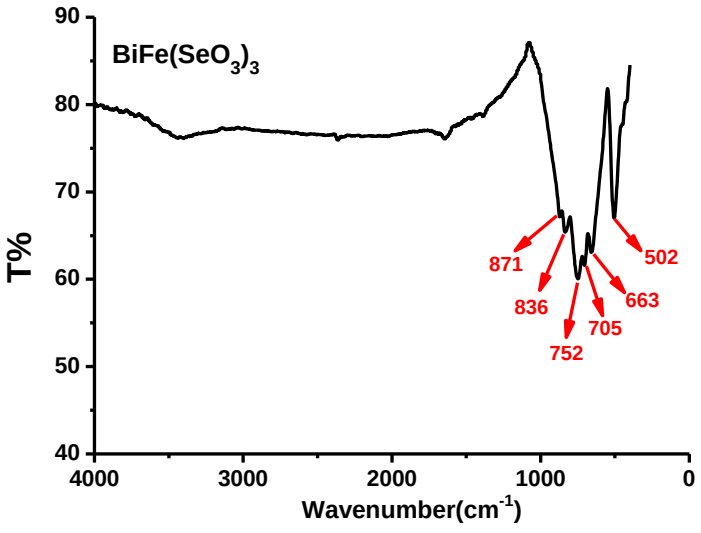

(e)

Figure S3. IR Spectra of $Pb_3(TeO_3)Cl_4$ (a), $Pb_3(SeO_3)_2Br_2$ (b), $Pb_2Cd_3(SeO_3)_4I_2(H_2O)$ (c), $Pb_2Ge(SeO_3)_4$ (d) and $BiFe(SeO_3)_3$ (e).

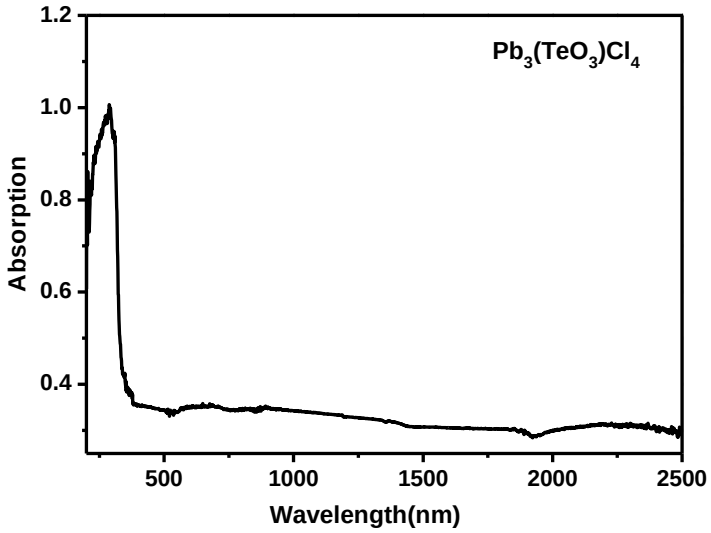

(a)

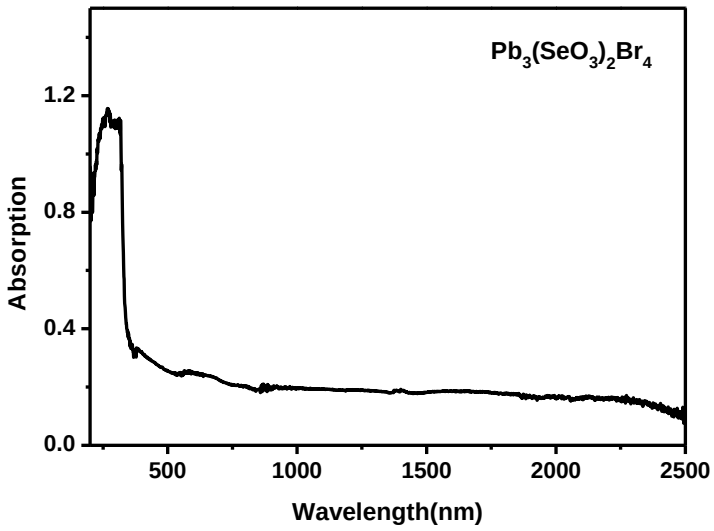

(b)

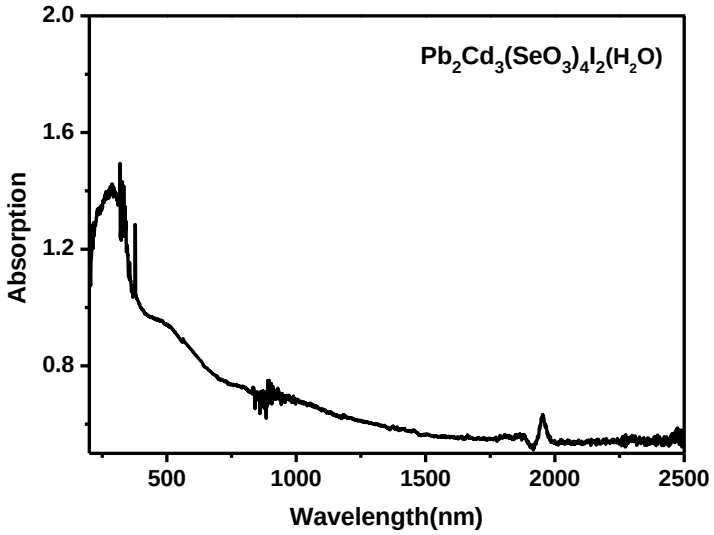

(c)

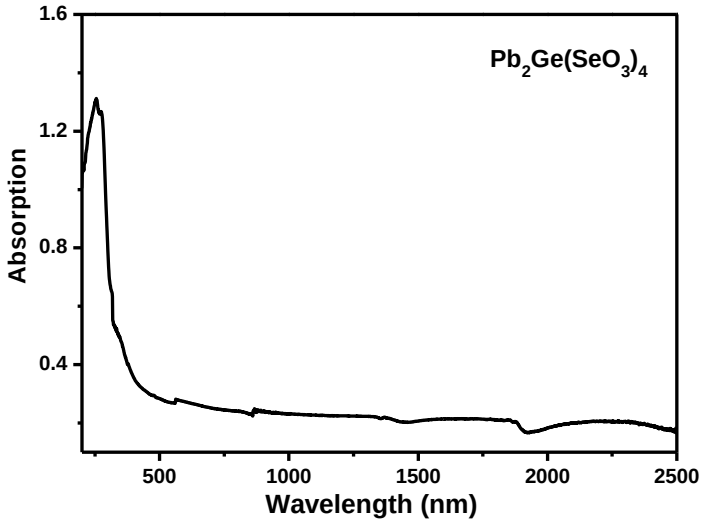

(d)

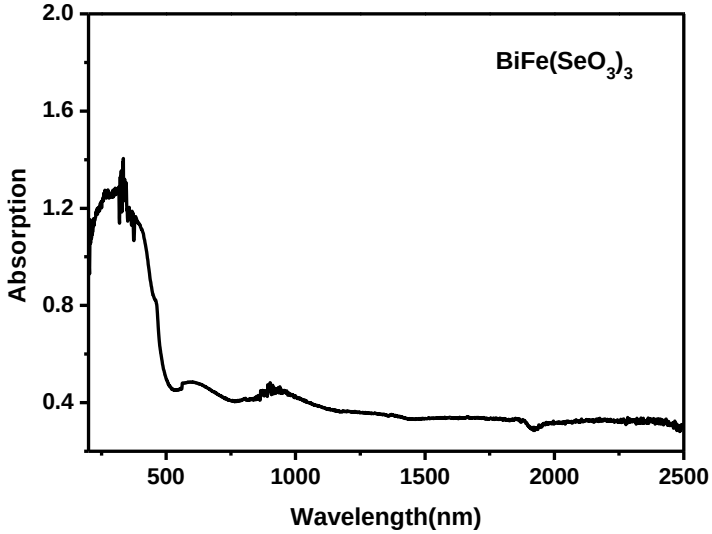

(e)

Figure S4. Absorption spectra of $Pb_3(TeO_3)Cl_4$ (a), $Pb_3(SeO_3)_2Br_2$ (b), $Pb_2Cd_3(SeO_3)_4I_2(H_2O)$ (c), $Pb_2Ge(SeO_3)_4$ (d) and $BiFe(SeO_3)_3$ (e).

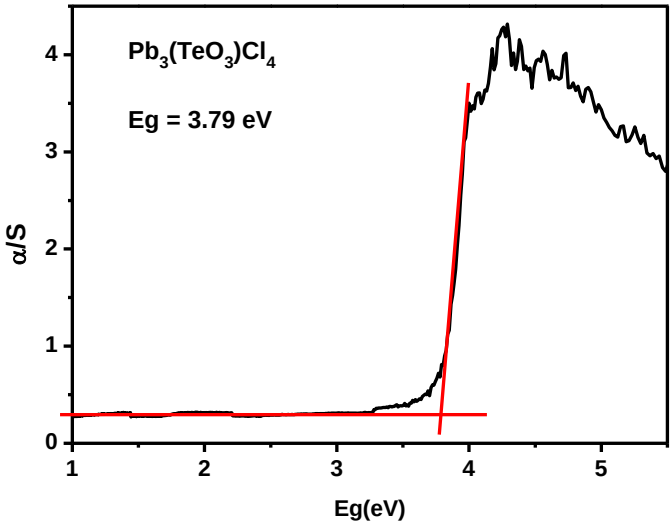

(a)

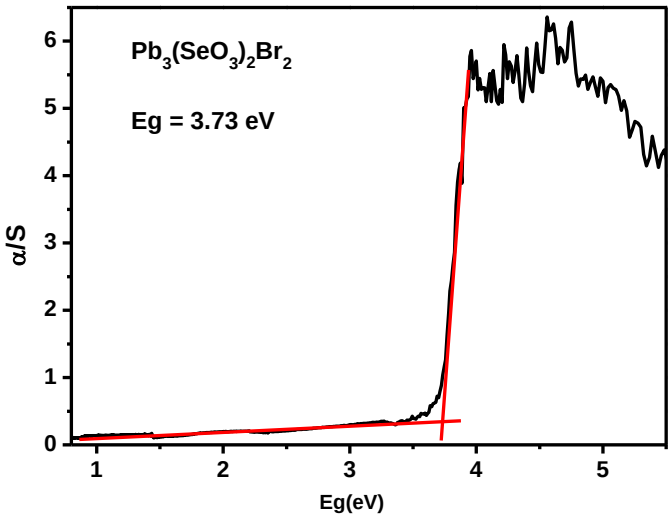

(b)

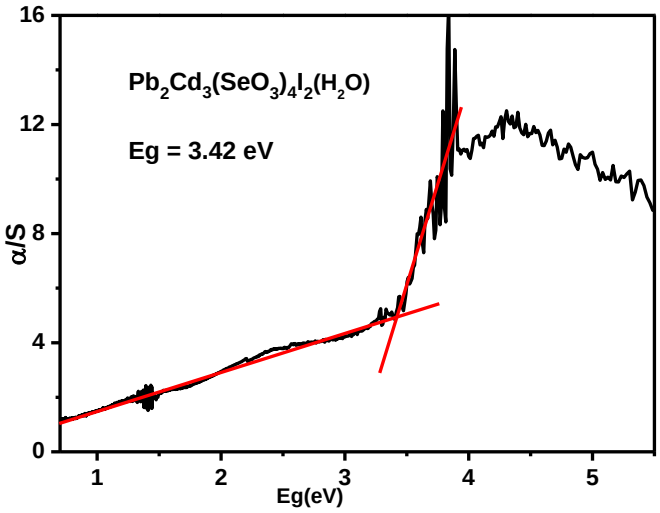

(c)

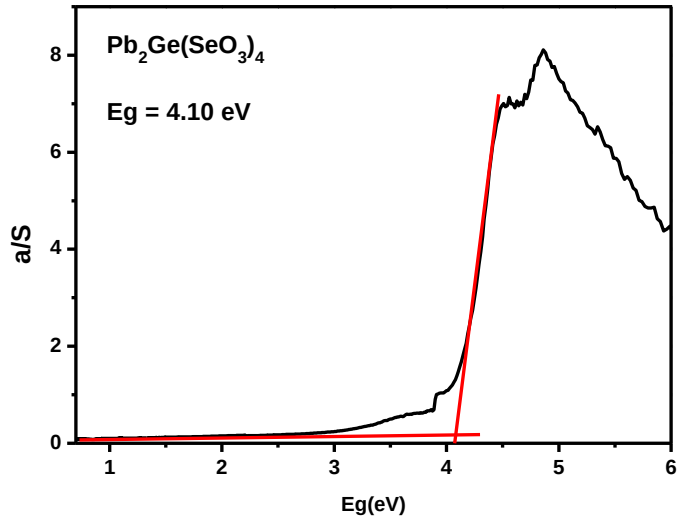

(d)

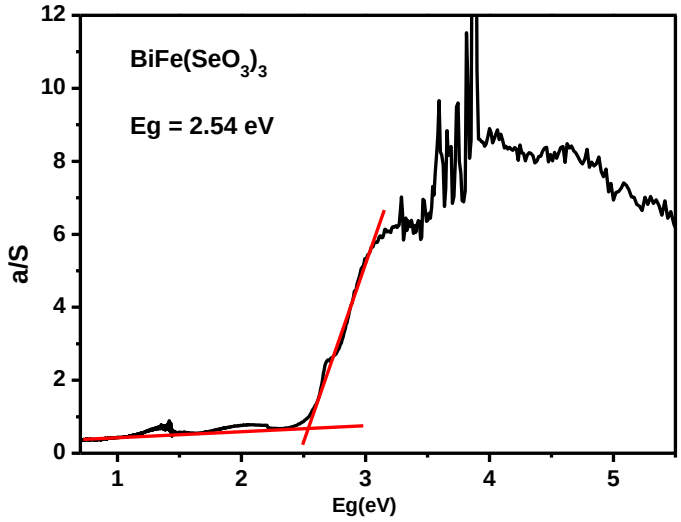

(e)

Figure S5. Optical diffuse reflectance spectra of $Pb_3(TeO_3)Cl_4$ (a), $Pb_3(SeO_3)_2Br_2$ (b), $Pb_2Cd_3(SeO_3)_4I_2(H_2O)$ (c), $Pb_2Ge(SeO_3)_4$ (d) and $BiFe(SeO_3)_3$ (e).

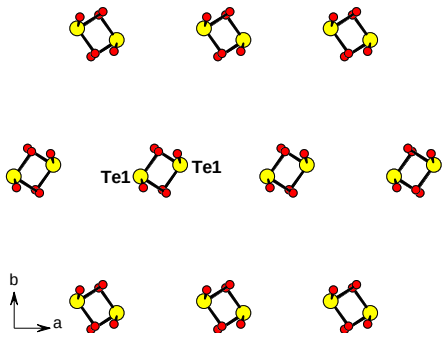

(a)

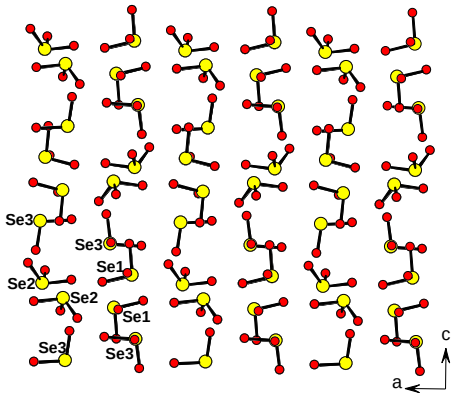

(b)

Figure S6. The orientations of the TeO_3 in $Pb_3(TeO_3)Cl_4$ and that of SeO_3 in $BiFe(SeO_3)_3$.

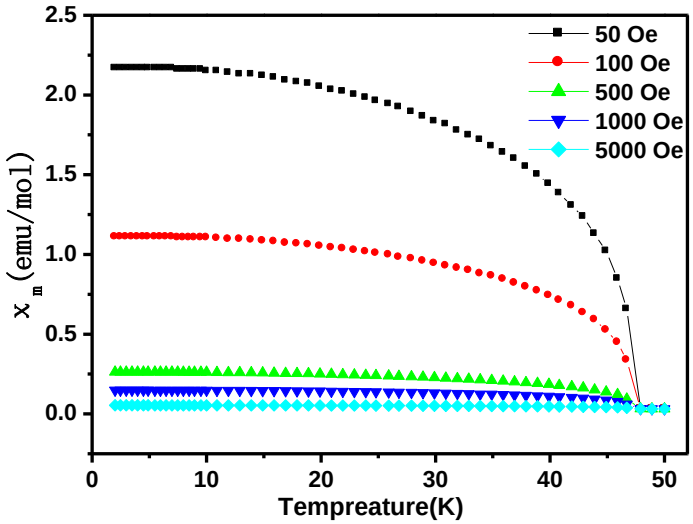

(a)

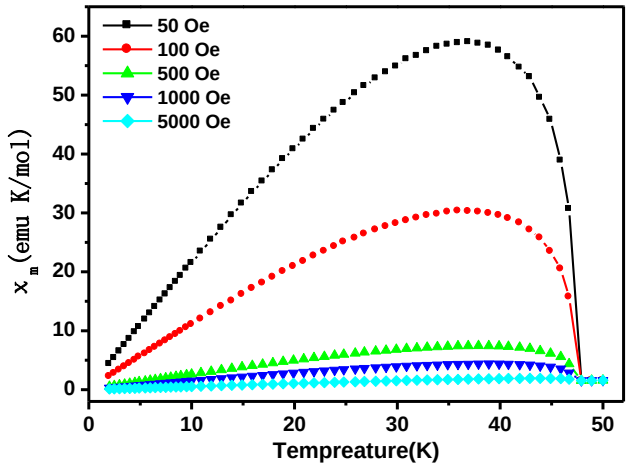

(b)

Figure S7. Plots of χ_M *vs.* T (a) and $\chi_M T$ *vs.* T (b) at various fields in 2-50 K.

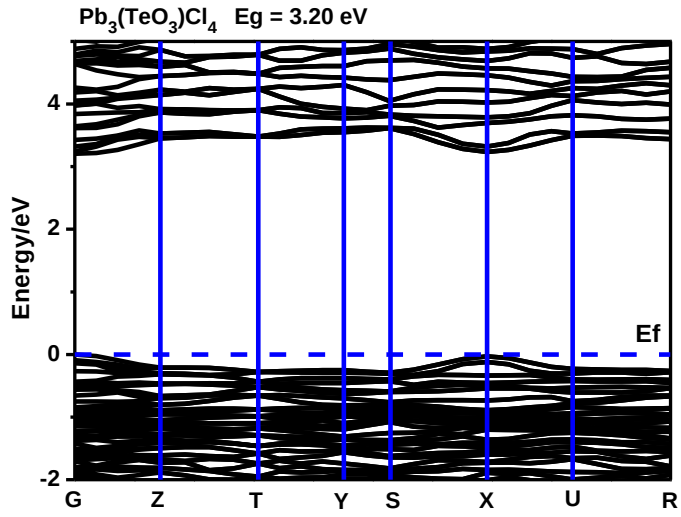

(a)

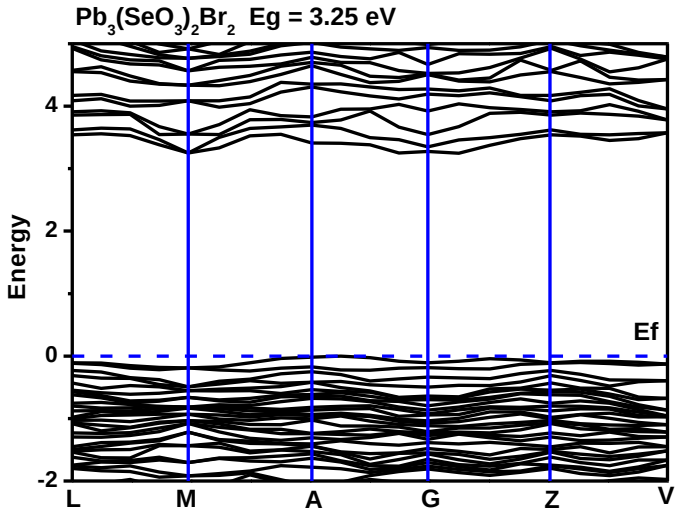

(b)

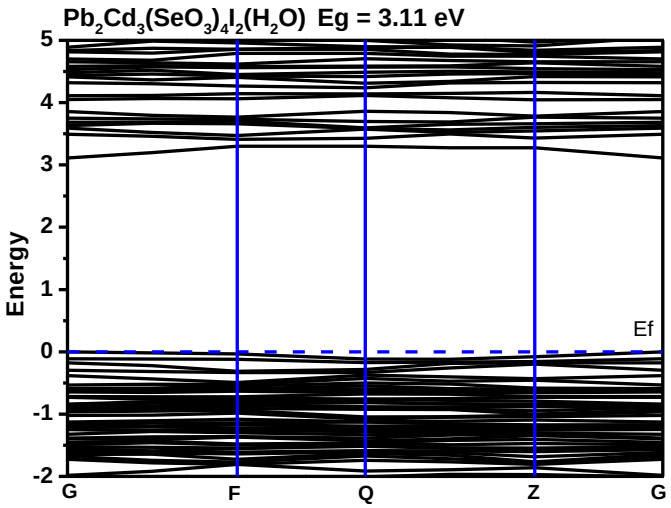

(c)

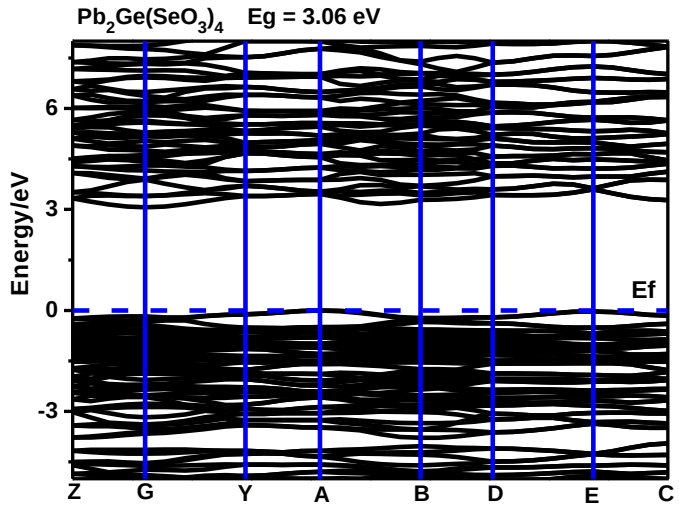

(d)

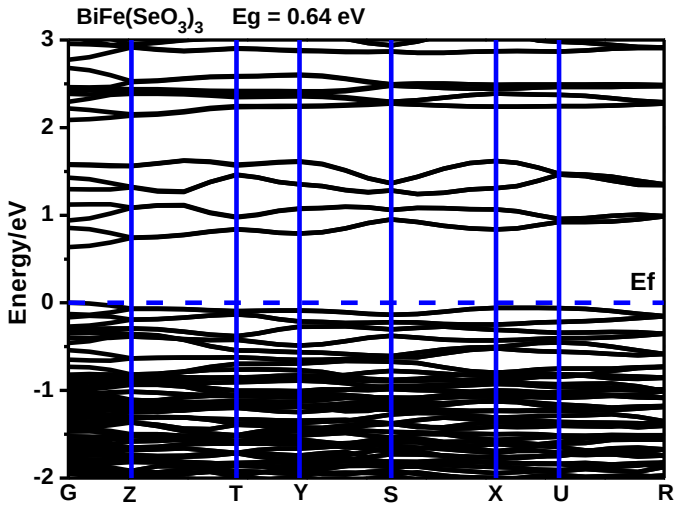

(e)

Figure S8. Band structures for $Pb_3(TeO_3)Cl_4$ (a), $Pb_3(SeO_3)_2Br_2$ (b), $Pb_2Cd_3(SeO_3)_4I_2(H_2O)$ (c), $Pb_2Ge(SeO_3)_4$ (d) and $BiFe(SeO_3)_3$ (e). The Fermi level is set at 0 eV.

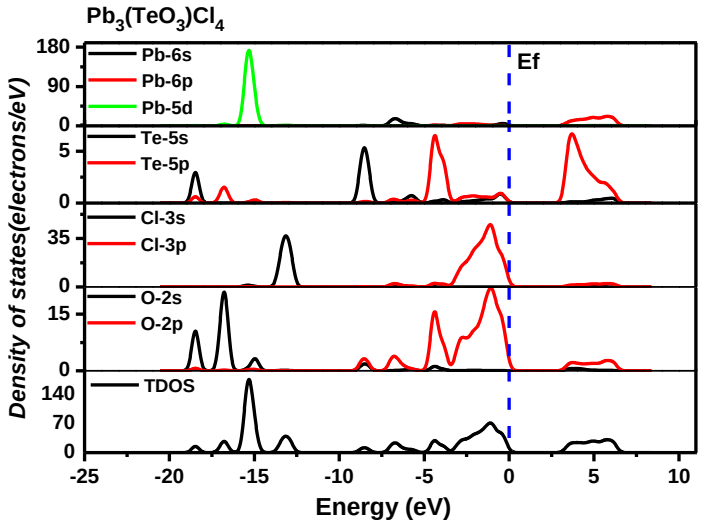

(a)

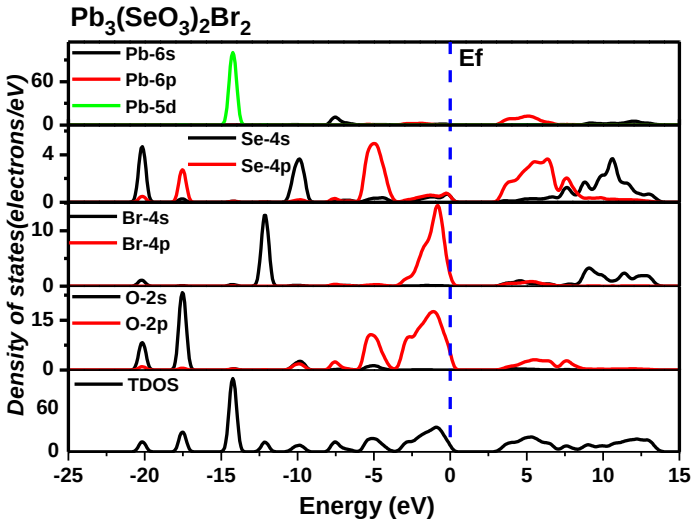

(b)

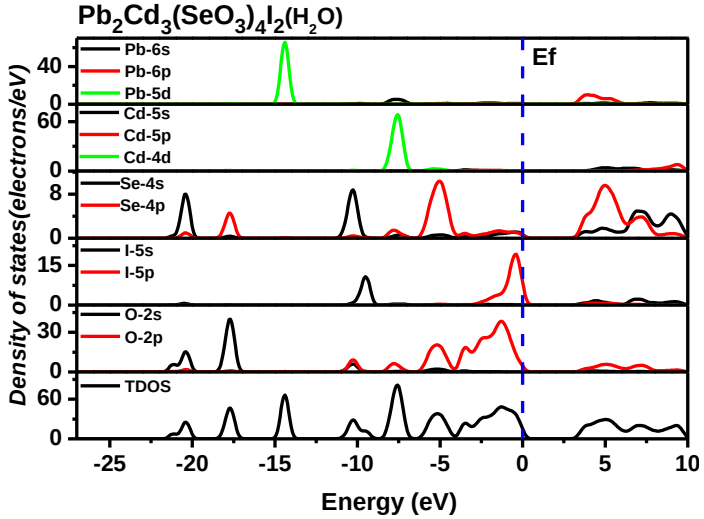

(c)

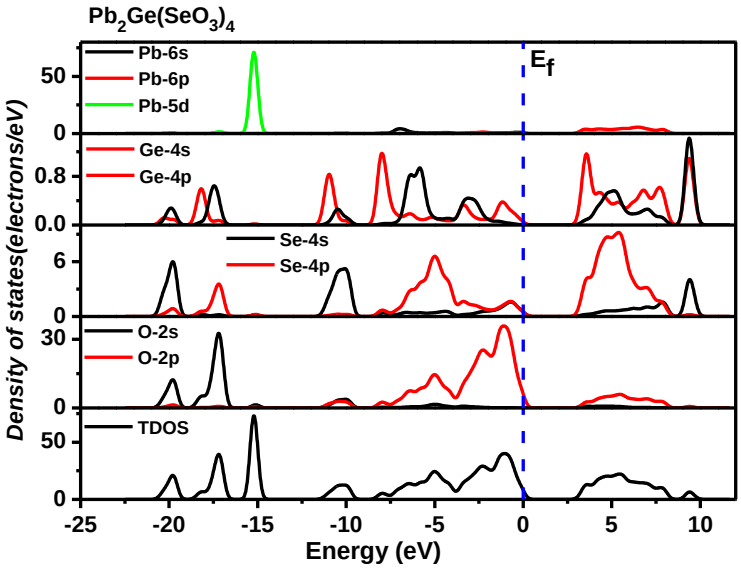

(d)

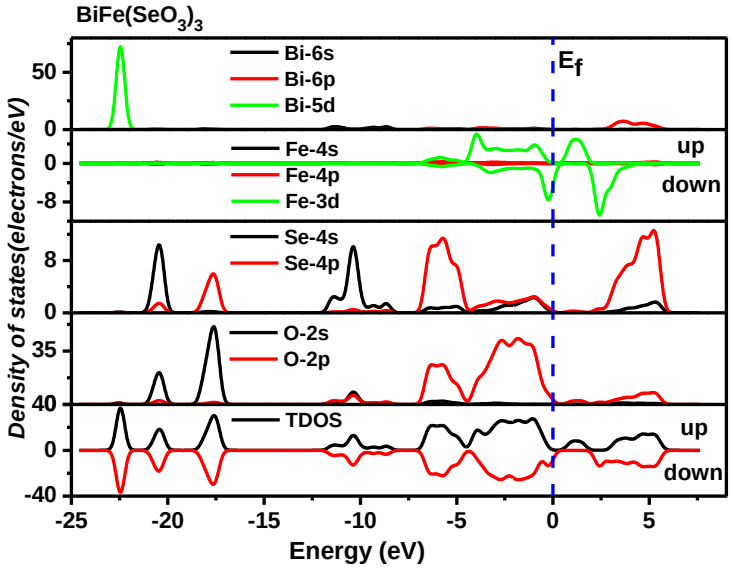

(e)

Figure S9. Total density of states and partial density of states of $Pb_3(TeO_3)Cl_4$ (a), $Pb_3(SeO_3)_2Br_2$ (b), $Pb_2Cd_3(SeO_3)_4I_2(H_2O)$ (c), $Pb_2Ge(SeO_3)_4$ (d) and $BiFe(SeO_3)_3$ (e). The Fermi level is set at 0 eV.

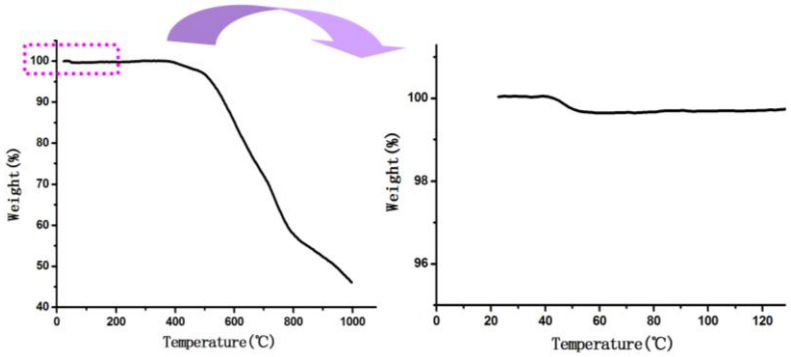

Figure S10. The TGA diagram of $Pb_2Cd_3(SeO_3)_4I_2(H_2O)$ (left) and the enlarged TGA diagram between 30-120 °C (right).